Chang Yunhua (Orcid ID: 0000-0002-1622-5330)

Huang Ru-Jin (Orcid ID: 0000-0002-4907-9616)

Ge Xinlei (Orcid ID: 0000-0001-9531-6478)

Puzzling haze events in China during the coronavirus (COVID-19) shutdown

Yunhua Chang,[1] Ru-Jin Huang,[2] Xinlei Ge,[3] Xiangpeng Huang,[3] Jianlin Hu,[3] Yusen Duan,[4] Zhong Zou,[5] Xuejun Liu,[6] and Moritz F. Lehmann.[7]

[1]Yale-NUIST Center on Atmospheric Environment, Nanjing University of Information Science & Technology, Nanjing 210044, China

[2]State Key Laboratory of Loess and Quaternary Geology, Center for Excellence in Quaternary Science and Global Change, and Key Laboratory of Aerosol Chemistry & Physics, Institute of Earth and Environment, Chinese Academy of Sciences, Xi'an 710061, China

[3]School of Environmental Science and Engineering, Nanjing University of Information Science & Technology, Nanjing 210044, China

[4]Shanghai Environmental Monitoring Center, Shanghai 200030, China

[5]Department of Environmental Science & Engineering, Fudan University, Shanghai 200433, China

This article has been accepted for publication and undergone full peer review but has not been through the copyediting, typesetting, pagination and proofreading process which may lead to differences between this version and the Version of Record. Please cite this article as doi: 10.1029/2020GL088533

[6]College of Resources & Environmental Sciences, China Agricultural University, Beijing 100193, China

[7] Department of Environmental Sciences, University of Basel, Basel 4056, Switzerland

Corresponding authors: Ru-Jin Huang (rujin.huang@ieecas.cn; ORCID: 0000-0002-4907-9616) and Yunhua Chang (changy13@nuist.edu.cn; ORCID: 0000-0002-1622-5330).

Key Points:

- Higher concentrations and distinct compositions of aerosol particles were observed during the COVID-19 shutdown
- Fast formation of secondary inorganic aerosol contributed to high aerosol mass loading
- Longer-range, regional transport facilitated and enhanced particulate nitrate formation

Abstract

It is a puzzle as to why more severe haze formed during the New Year Holiday in 2020 (NYH-20), when China was in an unprecedented state of shutdown to contain the coronavirus (COVID-19) outbreak, than in 2019 (NYH-19). We performed a comprehensive measurement and modeling analysis of the aerosol chemistry and physics at multiple sites in China (mainly in Shanghai) before, during, and after NYH-19 and NYH-20. Much higher secondary aerosol fraction in $PM_{2.5}$ were observed during NYH-20 (73%) than during NYH-19 (59%). During NYH-20, $PM_{2.5}$ levels correlated significantly with the oxidation ratio of nitrogen ($r^2 = 0.77$, $p < 0.01$), and aged particles from northern China were found to impede atmospheric new particle formation and growth in Shanghai. A markedly enhanced efficiency of nitrate aerosol formation was observed along the transport pathways during NYH-20, despite the overall low atmospheric NO_2 levels.

Plain Language Summary

In China, there are multiple cases (e.g., the 2008 Summer Olympics in Beijing and the 2010 World Expo in Shanghai) when combustion-related emissions (e.g., NO_x) were actively, and successfully, reduced to transiently improve air quality. During the extended Chinese Lunar New Year holiday in 2020 (between 24 January and 10 February), whole China was in an unprecedented state of shutdown, because most people were contained in their homes to reduce the spread of the novel coronavirus disease (COVID-19). Mobility, energy demand and industrial output remained far below their normal levels. Nevertheless, widespread haze pollution still occurred over Eastern China. To elucidate haze formation mechanisms, we performed comprehensive and continuous measurements of aerosol chemistry and physics in

and out of Shanghai before, during, and after the Chinese New Year Holiday in 2019 and 2020, respectively. We argue that the synergistic effects of long-range transport and atmospheric chemistry leading to the efficient conversion of NO_x to particulate nitrate were the key of haze formation during the Chinese New Year Holiday of the COVID-19 outbreak in Shanghai.

1 Introduction

In the first half December 2019, several cases of pneumonia with unknown aetiology were reported in Wuhan City, Hubei Province, China (Zhu et al., 2020; Wu et al., 2020a). On 7 January 2020, a novel coronavirus called 2019-nCoV was identified as the cause of such pneumonia by the Chinese Center for Disease Control (Huang et al., 2020a; Wu and McGoogan, 2020). The World Health Organization (WHO) declared the outbreak to be a Public Health Emergency of International Concern, and on 11 February 2020 announced "COVID-19" to be the official name of the novel coronavirus disease (Sohrabi et al., 2020). On 23 January, a day before the Lunar New Year of 2020, China's central government imposed a lockdown in Wuhan and other cities in the Hubei province in an effort to quarantine the epicenter of the COVID-19 outbreak (Wu et al., 2020b). However, the epidemic outbreak in the Hubei province happened concurrent with the Spring Festival travel rush, with ~5 million people migrating to other regions, just before the lockdown of Wuhan, aiding the spread of COVID-19 over most of China (Chen et al., 2020).

Facing the great challenge of the fast-spreading virus, all local governments raised their infectious disease response activities to the highest alert levels. The 2020 Chinese New Year Holiday (NYH-20) was planned originally for the week from January 24 to January 30. To

better control the epidemic, and to extenuate the transportation demands, China expanded NYH-20 to February 10 (18 days totally) (China, 2020). Quarantines, blocked roads and checkpoints throughout the country's urban and rural areas forced most people to stay at home. The measures taken during NYH-20 were, and still are, dramatically affecting the country's economy (Warwick and Roshen, 2020). The energy demand and industrial output remained far below the average levels of the same periods in preceding years. For example, energy production by coal-fired power plants was reduced by one third. Oil refineries and steel industries reached the lowest activity level of the past five years. Also, vehicular transportation and domestic flights were reduced by > 70% during NYH-20 (Myllyvirta, 2020).

The reduction in industrial coal and oil combustion was associated with a significant decrease in the emissions of combustion-derived air pollutants (e.g., NO_x and SO_2) (Myllyvirta, 2020). Quite surprisingly, severe haze pollution with high $PM_{2.5}$ mass concentrations were nevertheless observed over Eastern China (Wang, 2020). As one of the largest megacities in China, Shanghai pioneered the implementation of a series of control measures against the spread of infections during the COVID-19 outbreak in early 2020 (Perman, 2020), providing an unprecedent opportunity to understand this haze paradox, i.e., the elevation of atmospheric $PM_{2.5}$ concentrations despite lower emissions. In this study, we present results from analyses of aerosol chemistry and physics performed at an urban site in Shanghai before, during, and after the New Year Holiday in 2019 (NYH-19) and 2020 (NYH-20), and we compared the chemical composition and formation processes of the aerosols, as well as meteorological conditions, between the two periods in order to gain clues on the haze event puzzle in NYH-20.

2 Materials and Methods

2.1 Site description

The Pudong site (PD; 31.233°N, 121.545°E; 15 m a.g.l) represents an urban setting in central Shanghai (Chang et al., 2016). The measurements were conducted before (from 12 January to 3 February 2019 and, from 1 January to 23 January 2020), during (from 4 February to 10 February 2019 and, from 24 January to 10 February 2020), and after (from 11 February to 26 February 2019 and, from 11 February to 26 February 2020) the New Year Holidays in 2019 (NYH-19) and 2020 (NYH-20). During NYH-20, additional, more sporadic, measurements conducted at other sampling sites were included to support our main campaign at PD: Dongtan Eco-park (DT; 31.524°N, 121.958°E) and Dianshan Lake (DSH; 31.096°N, 120.988°E) in rural Shanghai, Caochangmen in urban Nanjing City (32.057°N, 118.749°E; Jiangsu Province), Shanxi in rural Jiaxing City (30.854°N, 120.899°E; Zhejiang Province), and the Tieta branch of the Institute of Atmospheric Physics in urban Beijing City (39.974°N, 116.371°E). Detailed site descriptions are available in our previous work (Jiang et al., 2015; Chang et al., 2020).

2.2 Field measurements

Inorganic components of $PM_{2.5}$ (NH_4^+, NO_3^-, SO_4^{2-}, Cl^-, Na^+, K^+, Ca^{2+}, Mg^{2+}) and water-soluble gases (NH_3, SO_2, HCl, HONO and HNO_3) were assessed at the sites in Shanghai, Jiaxing, and Nanjing using a semi-continuous Monitoring device for AeRosols and Gases in ambient Air (MARGA 2060; Metrohm Applikon B.V.; Delft, Netherland) at hourly time resolution (Chang et al., 2020). At the PD site in Shanghai, $PM_{2.5}$ inorganic species, NH_3

concentrations, temperature and relative humidity (RH) were used to calculate the aerosol water content (AWC) using the ISORROPIA-II model (Fountoukis and Nenes, 2007). In Beijing, an Aerodyne Time-of-Flight-Aerosol Chemical Speciation Monitor (ToF-ACSM) was used, equipped with a $PM_{2.5}$ aerodynamic lens and capture vaporizer that can measure nonrefractory $PM_{2.5}$ (NR-$PM_{2.5}$) aerosol species in real-time, including organics, NH_4^+, NO_3^-, SO_4^{2-}, and Cl^- (Sun et al., 2020). Simultaneously, mass concentrations of organic carbon (OC) and elemental carbon (EC) in $PM_{2.5}$ at PD were measured hourly, using a semi-continuous OC-EC analyzer (model RT-4; Sunset Laboratory Inc.; Tigard, USA) based on the thermal-optical technique and the NIOSH 5040 protocol (Chang et al., 2017). Organic matter (OM) was found to have an average OM/OC ratio of 1.5 in Shanghai (Huang et al., 2012b). The Minimum R Squared (MRS) method was used to estimate secondary organic carbon (SOC) concentrations based on the measured OC and EC data (Wu and Yu, 2016). Besides, mass concentrations of 19 elements (Si, Fe, K, Ca, Zn, Mn, Pb, Ba, V, Cu, Cd, As, Ni, Cr, Ag, Se, Hg, Co and Au) in $PM_{2.5}$ at PD were determined every hour by a multi-metal monitor (Xact™ 625; Cooper Environmental Services, LLT; Portland, USA) (Chang et al., 2018). To investigate atmospheric new particle formation at DSH and DT, two instruments, one nano-scanning mobility particle sizer (nano-SMPS) and one long-SMPS, were operated simultaneously at each site to measure number size distributions of 3-736 nm particles at a time resolution of 5 min (Yao et al., 2018). The performance/accuracy of these online instruments was validated in our previous work (Chang et al., 2016; 2017; 2018; 2019).

Additional measurements included the bulk $PM_{2.5}$ mass concentrations using a tapered element oscillating microbalance (TEOM) and a filter dynamics measurement system (FDMS)

(TEOM-FDMS 1405-F; Thermo Fisher Scientific™; Waltham, USA). RH, air temperature (*T*), atmospheric pressure, and wind speed and direction were recorded by a series of Vaisala® weather sensors (WXT530 Weather Transmitter Series; Vaisala®; Vantaa, Finland) at 10 min time resolution. The acquired original backscatter signals from ceilometer (CL51; Vaisala®; Vantaa, Finland) measurements were used to retrieve the cloud-base and planetary boundary layer height (PBLH) up to 15.4 km, at a time and space resolution of ~10 s and 10 m, respectively (Zhang et al., 2012; Peng et al., 2017). It needs to be noted that the PBLH values measured with the CL51 ceilometer in our study are relatively low, likely due to high aerosol loadings that affect the backscatter signals (Tang et al., 2015). As detailed in the Supplementary Information (Text S1), large biases have been found for PBLH values measured by different methods, including radiosonde, ground-based lidar, and Cloud-Aerosol Lidar with Orthogonal Polarization (CALIOP) (Kim et al., 2008; Korhonen et al., 2014; Ho et al., 2015; Liu et al., 2015; Liu et al., 2019; Zhang et al., 2016; Guo et al., 2019; Su et al., 2018).

2.3 Air quality modeling

Air quality in Shanghai and the surrounding Yangtze River Delta region during 1 January to 29 February 2020 was simulated using the Community Multiscale Air Quality Model (CMAQ) version 5.2. The anthropogenic air pollutant emissions were estimated by the Shanghai Academy of Environmental Sciences, and the emission reductions during the lockdown period were estimated using the online continuous stack emission monitoring data in Shanghai. Meteorological conditions were simulated with the Weather Research and Forecasting (WRF) Model version 4.0. The horizontal grid resolution was 4 km. The model

configurations of WRF and CMAQ, respectively were equivalent to the ones used in the study by Hu et al. (2016).

3 Results and Discussion

Time series data of major chemical components of $PM_{2.5}$ and their fractional contribution before, during, and after NYH-19 and NYH-20 are shown in Fig. 1. The average $PM_{2.5}$ concentrations decreased from 55.1 μg m^{-3} before NYH-19 to 29.8 μg m^{-3} during NYH-19, and then back to 42.2 μg m^{-3} after NYH-19 (Fig. 1a). This temporal pattern is expected, as it is consistent with the typical fluctuation of energy demand before, during and after the New Year Holidays. China relies on coal for over 60% of its energy consumption (Tang et al., 2019). The Chinese New Year Holidays represent officially a one-week national celebratory event. However, coal consumption typically starts to decline before the Chinese New Year, generally reaching its minimum during the holiday period before returning to its peak around half a month after the weeklong break (Huang et al., 2012a). In early 2020, the measures taken to minimize the spread of COVID-19 during NYH-20 have resulted in unprecedented and longer-lasting reductions in terms of social movement, transportation, energy demand and emissions. According to the urban travel intensity determined in Shanghai, the pre-holiday travel activity in 2020 was 26% higher than the year before but was more than 50% lower after the New Year of 2020 (Fig. S1). The nationwide reduction in automotive mobility and energy production following the COVID-19 outbreak was accompanied by plummeting atmospheric NO_2 levels. More precisely, satellite observations show that NO_2 emissions during the economic slowdown were reduced all over China to a record low, i.e., not only with respect to the pre-holiday period, but also when compared to the same holiday-week period following the 2019 Lunar New Year

(Fig. S2) (Myllyvirta, 2020; Compernolle and Lefever, 2020), which was consistent with the result of surface NO_2 measurement (Fig. S3).

The decline in NO_2 levels clearly coincided with the large reduction of coal consumption (Patel, 2020). NO_2 is a key contributor to smog and haze in the atmosphere. Therefore, if NO_2 emissions were to be the main factor governing air quality, the $PM_{2.5}$ concentrations during NYH-20 should also have been at minimum levels, yet this was not observed. Most curiously, frequent $PM_{2.5}$ spikes were observed during NYH-20 despite lower NO_2 and other emissions from industry and vehicles, and the overall $PM_{2.5}$ level during NYH-20 was more than 2.5 times higher than during NYH-19 (excluding a 12-h episode during the eve of Chinese New Year in 2019) (Fig. 1). Moreover, such apparently paradox haze events during NYH-20 also emerged in other megacities like Beijing (Wang, 2020).

In order to understand the mechanisms and conditions that may have resulted in the observed unusual low-emission/high-$PM_{2.5}$ scenario, we first compared the meteorological parameters during NYH-19 and NYH-20 and tested whether the meteorological conditions during NYH-20 were more conducive to haze pollution. PBLH plays a vital role in determining the vertical dispersion of air pollutants that are emitted from the Earth's surface (Su et al., 2018). We observed one period of high $PM_{2.5}$ pollution ($PM_{2.5} > 75$ μg m^{-3}) during NYH-19, and three of these events during NYH-20. The average PBLH (mean ± 1σ) for the three haze events during NYH-20 were 565 ± 189 m (from 4:00 January 28 to 12:00 January 30), 565 ± 91 m (from 0:00 to 7:00 January 31), and 538 ± 62 m (from 13:00 to 16:00 January 31), respectively, which were similar to that during NYH-19 (528 ± 87 m; from 0:00 to 10:00

February 4). Similar to observations by Liu et al. (2019), the $PM_{2.5}$ concentrations were weakly anti-correlated with PBLH (see Fig. S4). Yet, as discussed below, $PM_{2.5}$ concentrations can be, and likely were, also affected by regional transport and secondary aerosol formation. Other parameters (e.g., *T*, RH) indicate that the overall meteorological conditions during NYH-19 (6.5 ± 3.8 ºC; 80.5 ± 12.2%) were also similar to those during NYH-20 (6.7 ± 3.0 ºC; 75.8 ± 22.1%). As becomes evident in Fig. S5, there was no significant correlation between wind speed and $PM_{2.5}$ mass concentration, neither during NYH-19 nor during NYH-20. Therefore it is reasonable to conclude that wind speed is not a determinant factor to influence $PM_{2.5}$ pollution. As a consequence, we argue that it was not the meteorology that can explain the observed differences in haze pollution between NYH-19 and NYH-20, but that other factors must have an important effect on the increased aerosol particle formation during NYH-20.

We further investigated the chemical composition of $PM_{2.5}$ to understand the haze puzzle during NYH-20. As shown in Fig. 1a and b, the fraction of secondary aerosols during NYH-20 (72.5%) was significantly higher ($p < 0.01$) than that during NYH-19 (59.1%). More specifically, during NYH-19, OM was the dominant component in $PM_{2.5}$, while in other periods (including NYH-20), nitrate consistently represented the largest fraction. The sum of sulfate, nitrate, and ammonium (SNA) aerosols during NYH-20 (24.1 μg m^{-3}) was significantly higher ($p < 0.01$) than during NYH-19 (14.7 μg m^{-3}). Fig. 1c clearly shows that the fractional contributions of secondary aerosol increased with increasing $PM_{2.5}$ mass concentrations for all three periods in 2020 (up to 88%), and a generally similar pattern was observed for the three periods in 2019 (see supplementary data). Compared to the lowest-concentration $PM_{2.5}$ bins, the secondary fraction in the highest-concentration $PM_{2.5}$ bins increased steadily (by up to

27%), suggesting major contribution specifically of secondary aerosols in driving particulate pollution (Huang et al., 2014; Xin et al., 2015). Moreover, particulate pollution was largely driven by the formation of SNA aerosols. For example, during NYH-20, the fractional contribution of SNA increased from 41% in the lowest-concentration $PM_{2.5}$ bin to 72% in the highest-concentration $PM_{2.5}$ bin, whereas the corresponding contribution of secondary organic aerosols (SOA) decreased from 11% to 5%. The high contribution of SNA aerosols to high particulate pollution in the studied urban atmosphere could be due to the synergistic effects of emission, chemistry, and transport (An et al., 2019; Guo et al., 2014).

As discussed above, the SOA concentrations during NYH-20 (3.8 μg m^{-3}) and NYH-19 were quite similar (4.3 μg m^{-3}) (Figure 2a). In contrast, the SNA aerosol concentrations were over 1.6 times higher during NYH-20 (24.1 μg m^{-3}) than during NYH-19 (14.7 μg m^{-3}) (see Fig. 2a), despite the fact their precursors were 26.2% (NO_2), 32.1% (SO_2), and 9.3% (NH_3) lower after NYH-20 than after NYH-19. This observation is consistent with the significantly higher sulfur oxidation ratio (SOR=$n[SO_4^{2-}]/(n[SO_4^{2-}]+n[SO_2])$) and nitrogen oxidation ratio (NOR=$n[NO_3^-]/(n[NO_3]+ n[NO_2])$) (Ji et al., 2018) during NYH-20 (SOR = 0.50 ± 0.15 and NOR = 0.21 ± 0.13) compared to NYH-19 (SOR = 0.25 ± 0.10 and NOR = 0.14 ± 0.11), indicating more efficient formation of SNA aerosols during NYH-20. Both NOR and SOR were positively correlated with $PM_{2.5}$ mass, yet NOR displayed a much higher correlation coefficient than SOR (Fig. 2b). During NYH-20, with the overall increase of $PM_{2.5}$ mass concentration, SOR and NOR increased continuously. Most strikingly, for NOR we observed a 5-fold increase between low low-$PM_{2.5}$ samples and the high-$PM_{2.5}$ samples (Fig. 2c). Low temperatures and high RH during the wintertime are generally favorable for the formation of

SNA aerosols. Field measurements by others also revealed that aqueous-phase oxidation of SO_2 can be an important formation pathway of sulfate at high RH during haze events (Xue et al., 2019; Cheng et al., 2016). Moreover, the transformation of HNO_3 into particle phase is generally enhanced at high RH and low temperature conditions (Sun et al., 2015; Huang et al., 2020b). However, a uniform response, neither of NOR nor of SOR, to temperature and RH was not discernable (Fig. 2c). For example, with the increase of $PM_{2.5}$ concentration, SOR increased steadily from 0.53 to 0.85; while a corresponding change for temperature and RH was not observed. Similarly, despite a lower temperature, NOR stabilized at 0.55 at $PM_{2.5} > 75$ μg m^{-3}. Finally, if at all, the lower *T* and higher-RH environment as encountered during NYH-19 should have stimulated the formation of secondary inorganic aerosols and should have led to higher, and not lower $PM_{2.5}$ mass concentrations compared to NYH-20.

Here we further elucidate the effects of heterogeneous (aqueous) and photochemical processes on the nitrate and sulfate secondary aerosol formation. The WRF-CMAQ results show NO_2 and OH radical display a non-linear relationship (Fig. S6). With the decrease of NO_2, OH radical concentration increases (Fig. S6). We have also compared the diurnal cycle of OH radicals before and after the COVID-19 shutdown. As shown in Fig. S7, the daytime OH concentrations were much higher after the shutdown than before the shutdown, which can partly explain the enhanced formation of nitrate during NYH-20. Correlations between nitrate and sulfate as function of aerosol water content (AWC), or odd oxygen ($O_x = NO_2 + O_3$) during NYH-20 were investigated in Fig. 2d. While there was generally a good correlation between nitrate and sulfate aerosol mass concentrations ($r^2 = 0.55$), they both were rather independent of AWC and O_x. This finding is further supported by the fact that there was no significant

correlation between AWC/O_x and nitrate/sulfate, respectively (Fig. S8), and that the diurnal cycles of SNA species did not follow the diurnal patterns of AWC and O_x (Fig. S9). These results suggest that other factors (e.g., long-range transport) likely affect the formation of SNA.

Located in the atmospheric outflow from East Asia, Shanghai is a typical receptor city, receiving episodically highly polluted air masses from northern China during wintertime. During NYH-20, there were three distinct $PM_{2.5}$ pollution episodes (PE) with $PM_{2.5}$ mass concentration peaks occurring on January 28 (PE-1), February 3 (PE-2), and February 9 (PE-3) (Fig. 3a). For each PE, a 2-day back trajectory cluster analysis at 500 m is provided in Fig. 3c. The majority of the polluted air masses derived from northern China. This is particularly true for PE-1, when an aerosol layer (white rectangle in Fig. 3a) between 1500 and 2500 m, detected by lidar ceilometer, was transported from the upper to the lower atmospheric layer. During periods with transiently low $PM_{2.5}$ concentrations and chemical speciation (i.e., nitrate and sulfate) (e.g., January 26: $PM_{2.5}$ = 5 μg m^{-3}; February 6: $PM_{2.5}$ = 12 μg m^{-3}), air masses originated mainly from the open ocean (Fig. S10). Performing an air-mass back trajectory analysis for Shanghai, we divided the potential geographical origins into five regions (i.e., local, northern China, southern China, northeast sea, and southeast sea; Fig. S11). During NYH-20, 43.3% of the air masses arrived from northern mainland China, a region with intensive industries and miscellaneous air pollution sources (e.g., residential coal combustion for heating and cooling), while the corresponding share was only 4.2% during NYH-19 (Fig. 3b). In fact, over 88% of air masses in NYH-19 derived from the open sea. Typically, the frequent and strong influence of long-range transport (e.g., from norther China) will lead to the input of aged PM that can serve as condensation sinks, hindering atmospheric nucleation, and

subsequent growth of newly formed nano-sized particles (Yao et al., 2018). Simultaneously measured at the Dongtan Eco-park (DT) and Dianshanhu (DSH) sites in Shanghai, the number size distributions of 3-736 nm particles during NYH-20 are illustrated in Fig. 3d. There is evidence for one new particle formation event that occurred after PE-2 under relative clean-air conditions, yet no continuous and lasting size growth from the nucleation-mode particles was observed before any of the PEs. Although sensitive to ambient conditions (e.g., concentrations of gaseous precursors, temperature, and RH), the lack of nucleation may partly be explained by large condensation sinks of preexisting particles from long-range transport. Collectively, these results provide putative evidence that long-range transport was of critical importance to haze pollution during NYH-20.

We can use the longest-lasting pollution episode (PE-1) as a test case to investigate how long-range atmospheric transport increase SNA secondary aerosol mass concentrations, and in turn NOR and SOR. The time series of SNA concentrations and their gaseous precursors before (0:00-19:00 LT, January 27), during (20:00 LT, January 27 - 10:00 LT, January 31), and after (11:00 LT, January 31 - 0:00 LT, February 1) PE-1 at the PD site in Shanghai are shown in Fig. 4a, and NOR and SOR in and out of Shanghai for each period in Fig. 4b and Fig. S12, respectively. The "apparent" growth rates ($\mathrm{mean}_{\mathrm{min}}^{\mathrm{max}} \pm 1\sigma$) of nitrate aerosol particles before, during, and after PE-1 were $2.5_{1.6}^{4.4} \pm 0.8$, $18.3_{8.2}^{26.9} \pm 4.0$, and $6.3_{4.4}^{11.0} \pm 2.1$ μg m^{-3} h^{-1}, respectively. Sulfate, ammonium, and SO_2 also reached the highest growth rates during PE-1. In contrast, the average concentration of NO_2 during PE-1 (37.5 μg m^{-3}) was lower than before (55.7 μg m^{-3}) and after (39.0 μg m^{-3}) PE-1. The minimum NO_2 during PE-1 cannot be explained by low local NO_2 emissions. In fact, during PE-1, the NO_2 fluctuations correspond well with

observed changes in NO_3^- (r^2 = 0.71) (Fig. 4a), suggesting that the low NO_2 observed during PE-1 may be best explained by a highly efficient conversion of NO_2 to nitrate. At all the receptor sites (Jiaxing site in Zhejiang and DT, PD, and DSH sites in Shanghai), NOR was the highest during PE-1. Interestingly, during the phase after PE-1, NOR was the lowest at DT (0.19; remote wetland) in the NE, followed by PD (0.26; urban), DSH (0.40; rural), and Jiaxing (0.55; suburban) in the SW. This inter-city NOR gradient is consistent with the transport pathway of air masses and the associated oxidation of NO_2, as evidenced at the regional scale during PE-1 (see Fig. 4b). More specifically, following the regional transport pathway from north to south, NOR during PE-1 was the lowest in Beijing (0.24), then increased to 0.36 in Nanjing, and finally reached the highest values in Jiaxing and Shanghai. In contrast, NOR in Beijing was the highest before PE-1, and then gradually decreased to 0.24 during PE-1 and to 0.10 after PE-1. Given that Beijing is located in the source region of the North China Plain, the high NOR before the Shanghai PE-1 reflects the efficient conversion of NO_2 to nitrate during longer-term transport from the North. As a consequence, we further argue that the lowest NO_2 concentration observed during PE-1 indicates the highly efficient conversion of NO_2 to nitrate along the transport pathways. During the first day of PE-1, we observed a much higher average RH in Shanghai (76.6%) than that in Beijing (40.5%) (Fig. 4b). Moreover, the growth rates of nitrate during PE-1 correlated significantly with RH in Shanghai (r^2 = 0.56, $p < 0.01$; Fig. S13), highlighting the important role of RH in regulating nitrate formation during transport. SOR during PE-1 in Shanghai (0.73 at DT and DSH, 0.76 at PD) was not only much higher than in Beijing (0.38) and Nanjing (0.68), but also higher than in the southernmost Jiaxing (0.65) (Fig. S12), suggesting divergent transport and transformation of sulfate versus nitrate.

4 Conclusions

In this work, we present a timely investigation of China's haze puzzle in Shanghai in early 2020. Over two-times higher mass concentrations of fine particles were observed during the New Year Holiday and the contemporaneous COVID-19 outbreak, despite the record economic slowdown and associated decline in pollutant emissions from business, transportation, and industry. Fast formation of secondary inorganic (mostly nitrate) aerosols was identified as the main factor contributing to the relatively high atmospheric particle concentrations (> 80%). We show that particulate nitrate formation can be largely enhanced (with nitrate formation rates up to 27 $\mu g\ m^{-3}\ h^{-1}$) during lasting regional transport, suggesting that differential transport patterns, rather than local emissions, may be responsible for fluctuations in aerosol concentrations (e.g., NYH-19 vs NYH-20). The results of this study highlight that regional joint management efforts and control strategies are required to effectively clear China's air.

Acknowledgments

This study was supported by the National Natural Science Foundation of China (Grant nos. 41975166, 41925015, 41705100), the Provincial Natural Science Foundation of Jiangsu (Grant no. BK20170946), the special fund of State Key Joint Laboratory of Environment Simulation and Pollution Control (Grant no. 19K01ESPCT), and the Opening Project of Shanghai Key Laboratory of Atmospheric Particle Pollution and Prevention (LAP^3; Grant no. FDLAP19001). The associated data can be downloaded online (https://doi.org/10.5281/zenodo.3738768).

Note: The authors declare that they have no conflicting interest.

Reference

An, Z., Huang, R. J., Zhang, R., Tie, X., Li, G., Cao, J., … Ji, Y. (2019) Severe haze in northern China: A synergy of anthropogenic emissions and atmospheric processes. *Proceedings of the National Academy of Sciences, 116,* 8657-8666. https://doi.org/10.1073/pnas.1900125116, 2019.3

Analysis: Coronavirus has temporarily reduced China's CO_2 emissions by a quarter. https://www.carbonbrief.org/analysis-coronavirus-has-temporarily-reduced-chinas-co2-emissions-by-a-quarter (lass access: 7 March 2020)

Airborne nitrogen dioxide plummets over China. https://earthobservatory.nasa.gov/images/146362/airborne-nitrogen-dioxide-plummets-over-china (lass access: 7 March 2020)

Chang, Y., Zou, Z., Deng, C., Huang, K., Collett, J. L., Lin, J., & Zhuang, G. (2016). The importance of vehicle emissions as a source of atmospheric ammonia in the megacity of Shanghai. *Atmospheric Chemistry and Physics, 16,* 3577-3594. https://doi.org/10.5194/acp-16-3577-2016

Chang, Y., Deng, C., Cao, F., Cao, C., Zou, Z., Liu, S., … Zhang, Y. (2017). Assessment of carbonaceous aerosols in Shanghai, China – Part 1: Long-term evolution, seasonal variations, and meteorological effects. *Atmospheric Chemistry and Physics, 17*, 9945-9964. https://doi.org/10.5194/acp-17-9945-2017

Chang, Y., Huang, K., Xie, M., Deng, C., Zou, Z., Liu, S., & Zhang, Y. (2018). First long-term and near real-time measurement of trace elements in China's urban atmosphere: Temporal variability, source apportionment and precipitation effect. *Atmospheric Chemistry and Physics*, *18*, 11793-11812. https://doi.org/10.5194/acp-18-11793-2018

Chang, Y., Zou, Z., Zhang, Y., Deng, C., Hu, J., Shi, Z., … Collett, J. (2019). Assessing contributions of agricultural and non-agricultural emissions to atmospheric ammonia in a Chinese megacity. *Environmental Science & Technology, 53*, 1822-1833. https://doi.org/10.1021/acs.est.8b05984

Chang, Y., Clarisse, L., Van Damme, M., Tao, Y., Zou, Z., Dore, A. J., & Collett, J. L. (2020). Ammonia emissions from mudflats of river, lake, and sea. *ACS Earth and Space Chemistry*. https://doi.org/10.1021/acsearthspacechem.0c00017 (just accepted)

Chen, Z., Zhang, Q., Lu, Y., Zhang, X., Zhang, W., Guo, C., … Lu, J. (2020b). Distribution of the 2019-nCoV epidemic and correlation with population emigration from Wuhan, China. *medRxiv*. https://doi.org/10.1101/2020.02.10.20021r824 (just accepted)

Cheng, Y., Zheng, G., Wei, C., Mu, Q., Zheng, B., Wang, Z., … Su, H. (2016). Reactive nitrogen chemistry in aerosol water as a source of sulfate during haze events in China. *Science Advances*. *2*. https://doi.org/10.1126/sciadv.1601530

The State Council's announcement on the arrangement of public holidays in 2020. http://www.gov.cn/zhengce/content/2019-11/21/content_5454164.htm (last access: 7 March 2020)

Fountoukis, C. & Nenes, A. (2007). ISORROPIA II: a computationally efficient thermodynamic equilibrium model for K^+–Ca^{2+}–Mg^{2+}–NH_4^+–Na^+–SO_4^{2-}–NO_3^-–Cl^-–H_2O aerosols. *Atmospheric Chemistry and Physics, 7*, 4639-4659. https://doi.org/10.5194/acp-7-4639-2007

Guo, J., Li, Y., Cohen, J. B., Li, J., Chen, D., Xu, H., Liu, L., … Zhai, P. (2019). Shift in the temporal trend of boundary layer height in China using long-term (1979-2016) radiosonde data. *Geophysical Research Letters, 46*, 6080-6089. https://doi.org/10.1029/2019GL082666

Guo, S., Hu, M., Zamora, M. L., Peng, J., Shang, D., Zheng, J., … Zhang, R. (2014). Elucidating severe urban haze formation in China. *Proceedings of the National Academy of Sciences, 111*, 17373-17378. https://doi.org/10.1073/pnas.1419604111

Ho, S., Peng, L., Anthes, R. A., Kuo, Y. & Lin, H. C. (2015). Marine boundary layer heights and their longitudinal, diurnal, and interseasonal variability in the Southeastern Pacific using COSMIC, CALIOP, and radiosonde data. *Journal of Climate, 28*, 2856-2872. https://doi.org/10.1175/JCLI-D-14-00238.1

Hu, J., Chen, J., Qing, Q., & Zhang, H. (2016). One-year simulation of ozone and particulate matter in China using WRF/CMAQ modeling system. *Atmospheric Chemistry and Physics*, 16, 10333-10350. https://doi.org/10.5194/acp-16-10333-2016

Huang, C., Wang, Y., Li, X., Ren, L., Zhao, J., Hu, Y., … Cao, B. (2020a). Clinical features of patients infected with 2019 novel coronavirus in Wuhan, China. *The Lancet, 395*, 497-506, https://doi.org/10.1016/S0140-6736(20)30183-5

Huang, K., Zhuang, G., Lin, Y., Wang, Q., Fu, J. S., Zhang, R., … Fu, Q. (2012a). Impact of anthropogenic emission on air quality over a megacity – Revealed from an intensive atmospheric campaign during the Chinese Spring Festival. *Atmospheric Chemistry and Physics*, *12*, 11631-11645. https://doi.org/10.5194/acp-12-11631-2012

Huang, R. J., Zhang, Y., Bozzetti, C., Ho, K. F., Cao, J. J., Han, Y., … Prevot, A. S. (2014). High secondary aerosol contribution to particulate pollution during haze events in China. *Nature, 514*, 218-222. https://doi.org/10.1038/nature13774

Huang, R. J., He, Y., Duan, J., Li, Y., Chen, Q., Zheng, Y., … O'Dowd, C. D. (2020b). Contrasting sources and processes of particulate species in haze days with low and high relative humidity in wintertime Beijing. *Atmospheric Chemistry and Physics Discussions*. https://doi.org/0.5194/acp-2020-158 (under review)

Huang, X. F., He, L. Y., Xue, L., Sun, T. L., Zeng, L. W., Gong, Z. H., … Zhu, T. (2012b). Highly time-resolved chemical characterization of atmospheric fine particles during 2010 Shanghai World Expo. *Atmospheric Chemistry and Physics, 12*, 4897-4907. https://doi.org/10.5194/acp-12-4897-2012

Liu, J., Huang, J., Chen, B., Zhou, T., Yan, H., Jin, H., … Zhang, B. (2015). Comparisons of PBL heights derived from CALIPSO and ECMWF reanalysis data over China, *Journal of Quantitative Spectroscopy and Radiative Transfer, 153*, 102-112. https://doi.org/10.1016/j.jqsrt.2014.10.011

Liu, N., Zhou, S., Liu, C. & Guo, J. (2019). Synoptic circulation pattern and boundary layer structure associated with $PM_{2.5}$ during wintertime haze pollution episodes in Shanghai. *Atmospheric Research*, *228*, 186-195. https://doi.org/10.1016/j.atmosres.2019.06.001

Ji, Y., Qin, X., Wang, B., Xu, J., Shen, J., Chen, J., … Zhang, T. (2018). Counteractive effects of regional transport and emission control on the formation of fine particles: A case study during the Hangzhou G20 summit. *Atmospheric Chemistry and Physics*, *18*, 13581-13600. https://doi.org/10.5194/acp-18-13581-2018

Jiang, Q., Sun, Y. L., Wang, Z., and Yin, Y.: Aerosol composition and sources during the Chinese Spring Festival: Fireworks, secondary aerosol, and holiday effects. *Atmospheric Chemistry and Physics*, *15*, 6023-6034. https://doi.org/10.5194/acp-15-6023-2015

Kim, S., Berthier, S., Raut, J., Chazette, P., Dulac, F. & Yoon, S. (2008). Validation of aerosol and cloud layer structures from the space-borne lidar CALIOP using a ground-based lidar in Seoul, Korea. *Atmospheric Chemistry and Physics*, *8*, 3705-3720. https://doi.org/10.5194/acp-8-3705-2008

Korhonen, K., Giannakaki, E., Mielonen, T., Pfüller, A., Laakso, L., Vakkari, V., … Komppula, M. (2014). Atmospheric boundary layer top height in South Africa: Measurements with lidar and radiosonde compared to three atmospheric models, *Atmospheric Chemistry and Physics*, *14*, 4263-4278. https://doi.org/10.5194/acp-14-4263-2014

Peng, J., Grimmond, C. S. B., Fu, X., Chang, Y., Zhang, G., Guo, J., … Tan, J. (2017). Ceilometer-based analysis of Shanghai's boundary layer height (under rain- and fog-free conditions). *Journal of Atmospheric and Oceanic Technology*, *34*, 749-764. https://doi.org/10.1175/JTECH-D-16-0132.1

Perman, T. (2020). Coronavirus ghost town: Shanghai has changed since the outbreak, in: USA Today. https://www.usatoday.com/story/opinion/2020/02/18/covid-19-shanghai-has-become-coronavirus-ghost-town-column/4786720002/ (lass access: 7 March 2020)

Sohrabi, C., Alsafi, Z., O'Neill, N., Khan, M., Kerwan, A., Al-Jabir, A., … Agha, R. (2020). World Health Organization declares Global Emergency: A review of the 2019 novel coronavirus (COVID-19). *International Journal of Surgery*, *76*, 71-76. https://doi.org/10.1016/j.ijsu.2020.02.034

Su, T., Li, Z., & Kahn, R. (2018). Relationships between the planetary boundary layer height and surface pollutants derived from lidar observations over China: Regional pattern and influencing factors. *Atmospheric Chemistry and Physics*, *18*, 15921-15935. https://doi.org/10.5194/acp-18-15921-2018

Sun, Y., He, Y., Kuang, Y., Xu, W., Song, S., Ma, N., … Worsnop, D. R. (2020) Chemical differences between PM_1 and $PM_{2.5}$ in highly polluted environment and implications in air pollution studies. *Geophysical Research Letters*, *47*, e2019GL086288. https://doi.org/10.1029/2019GL086288

Sun, Y. L., Wang, Z. F., Du, W., Zhang, Q., Wang, Q. Q., Fu, P. Q., … Worsnop, D. R. (2015). Long-term real-time measurements of aerosol particle composition in Beijing, China: Seasonal variations, meteorological effects, and source analysis. *Atmospheric Chemistry and Physics*, *15*, 10149-10165. https://doi.org/10.5194/acp-15-10149-2015

Tang, G., Zhu, X., Hu, B., Xin, J., Wang, L., Münkel, C., … Wang, Y. (2015). Impact of emission controls on air quality in Beijing during APEC 2014: Lidar ceilometer

observations. *Atmospheric Chemistry and Physics, 15,* 12667-12680. https://doi.org/10.5194/acp-15-12667-2015

Tang, L., Qu, J., Mi, Z., Bo, X., Chang, X., Anadon, L. D., … Zhao, X. (2019). Substantial emission reductions from Chinese power plants after the introduction of ultra-low emissions standards. *Nature Energy, 4,* 929-938. https://doi.org/10.1038/s41560-019-0468-1

Wang, O. (2020). China's capital shrouded in air pollution despite reduced emissions from coronavirus economic slowdown, in: South China Morning Post. https://www.scmp.com/economy/china-economy/article/3050527/chinas-capital-shrouded-air-pollution-despite-reduced (last access: 7 March 2020)

Wu, C., & Yu, J. Z. (2016). Determination of primary combustion source organic carbon-to-elemental carbon (OC/EC) ratio using ambient OC and EC measurements: secondary OC-EC correlation minimization method. *Atmospheric Chemistry and Physics, 16,* 5453-5465, 10.5194/acp-16-5453-2016

Wu, F., Zhao, S., Yu, B., Chen, Y. M., Wang, W., Song, Z. G., … Zhang, Y. Z. (2020a). A new coronavirus associated with human respiratory disease in China. *Nature,* . https://doi.org/10.1038/s41586-020-2008-3

Wu, J., Gamber, M., & Sun, W. (2020b). Does Wuhan need to be in lockdown during the Chinese Lunar New Year?. *International Journal of Environmental Research and Public Health, 17,* 1002. https://doi.org/10.3390/ijerph17031002

Wu, Z., Hu, M., Liu, S., Wehner, B., Bauer, S., Maßling, A., … Kulmala, M. (2007). New particle formation in Beijing, China: Statistical analysis of a 1-year data set. *Journal of Geophysical Research: Atmospheres, 112*. https://doi.org/10.1029/2006JD007406

Xin, J., Wang, Y., Pan, Y., Ji, D., Liu, Z., Wen, T., … Wang, L. (2015). The campaign on atmospheric aerosol research network of China: CARE-China. *Bulletin of the American Meteorological Society, 96,* 1137-1155. https://doi.org/10.1175/bams-d-14-00039.1

Xue, J., Yu, X., Yuan, Z., Griffith, S. M., Lau, A. K. H., Seinfeld, J. H., & Yu, J. Z. (2019). Efficient control of atmospheric sulfate production based on three formation regimes. *Nature Geoscience, 12,* 977-982. https://doi.org/10.1038/s41561-019-0485-5

Yao, L., Garmash, O., Bianchi, F., Zheng, J., Yan, C., Kontkanen, J., Junninen, H., … Wang, L. (2018). Atmospheric new particle formation from sulfuric acid and amines in a Chinese megacity. *Science, 361,* 278-281. https://doi.org/10.1126/science.aao4839

Zhang, C., Wang, Y., Lauer, A., Hamilton, K., & Xie, F. (2012). Cloud base and top heights in the Hawaiian region determined with satellite and ground-based measurements. *Geophysical Research Letters, 39*. https://doi.org/10.1029/2012GL052355

Zhang, W., Guo, J., Miao, Y., Liu, H., Zhang, Y., Li, Z. & Zhai, P. (2016). Planetary boundary layer height from CALIOP compared to radiosonde over China. *Atmospheric Chemistry and Physics, 16,* 9951-9963. https://doi.org/10.5194/acp-16-9951-2016

Zhu, N., Zhang, D., Wang, W., Li, X., Yang, B., Song, J., … Tan, W. (2020). A Novel Coronavirus from patients with pneumonia in China, 2019. *New England Journal of Medicine, 382,* 727-733. https://doi.org/10.1056/NEJMoa2001017

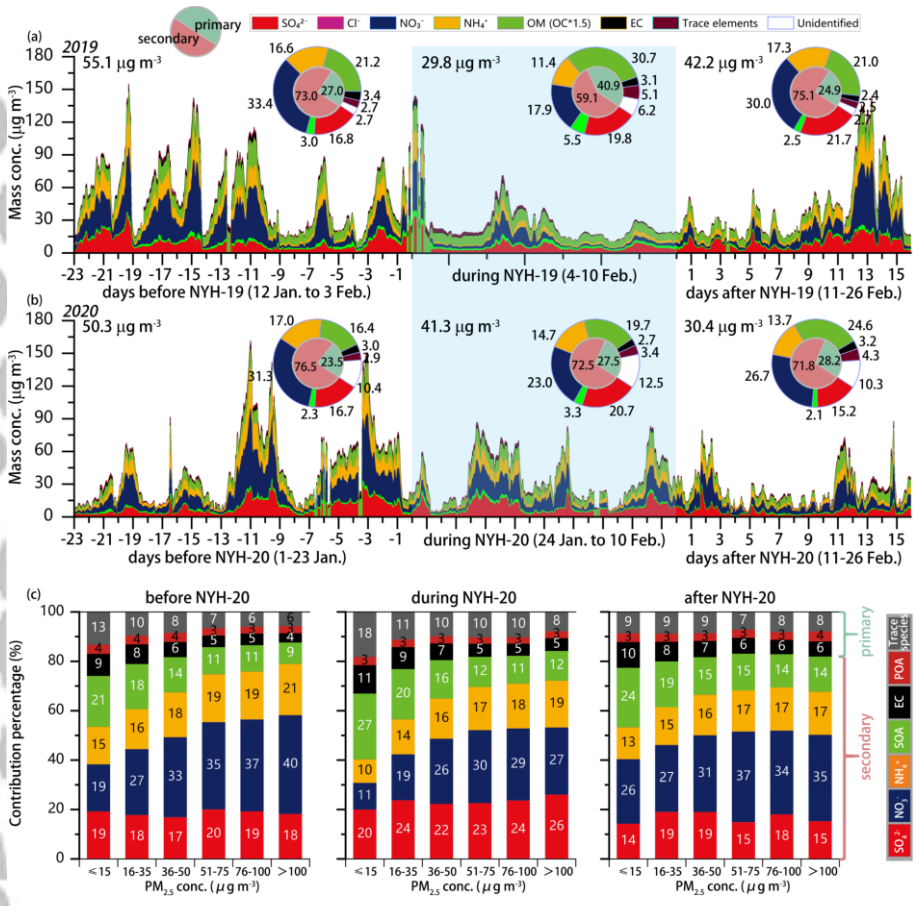

Figure 1. Time series of the major chemical components of $PM_{2.5}$ and fractional contributions before, during, and after the New Year Holiday in 2019 (a) and 2010 (b) measured at the Shanghai station PD. The numbers in the single panels (in μg m^{-3}) refer to the average $PM_{2.5}$ concentrations measured during each period. The fractional contributions as a function of the $PM_{2.5}$ bins before, during, and after NYH-20 are also shown (c). Note the uniform increase in the relative abundance of secondary aerosols with the increase of $PM_{2.5}$.

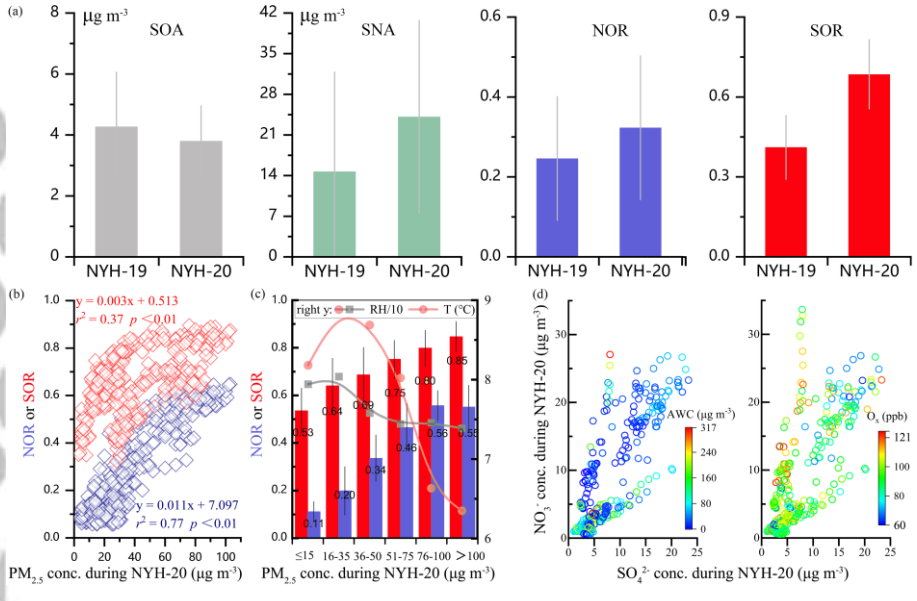

Figure 2. (a) Comparison of SOA (secondary organic aerosols), SNA (sulfate, nitrate, and ammonium aerosols), NOR (nitrogen oxidation ratio), and SOR (sulfur oxidation ratio) between NYH-19 and NYH-20. (b) Correlations between $PM_{2.5}$ concentration and NOR or SOR during NYH-20. (c) Variations of NOR, SOR, RH/10, and temperature as a function of $PM_{2.5}$ concentration during NYH-20. Each error bar indicates two standard deviations. (d) Correlations between sulfate and nitrate for different AWC and O_x concentrations during NYH-20.

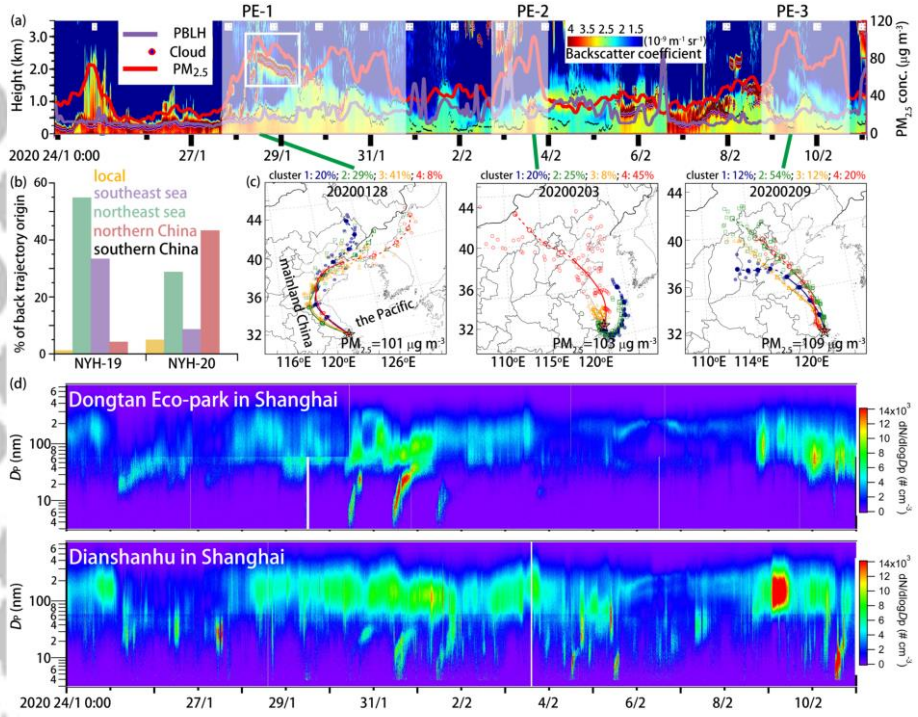

Figure 3. (a) Time series of attenuated backscatter density together with PBLH (purple line) and $PM_{2.5}$ mass concentration (red line) measured at PD during NYH-20. The white frame in (a) indicates the formation of an aerosol layer. The translucent rectangles represent $PM_{2.5}$ pollution episodes. (b) Airmass source apportioning in Shanghai based on air-mass back trajectory analysis during NYH-19 and NYH-20. The expression of the date is yyyymmdd. (c) HYSPLIT 2-day back trajectory cluster analysis at PD in Shanghai with an arriving height of 500 m for each $PM_{2.5}$ pollution peak. (d) Time series of particle number size distributions measured during NYH-20 at DT and DSH in Shanghai.

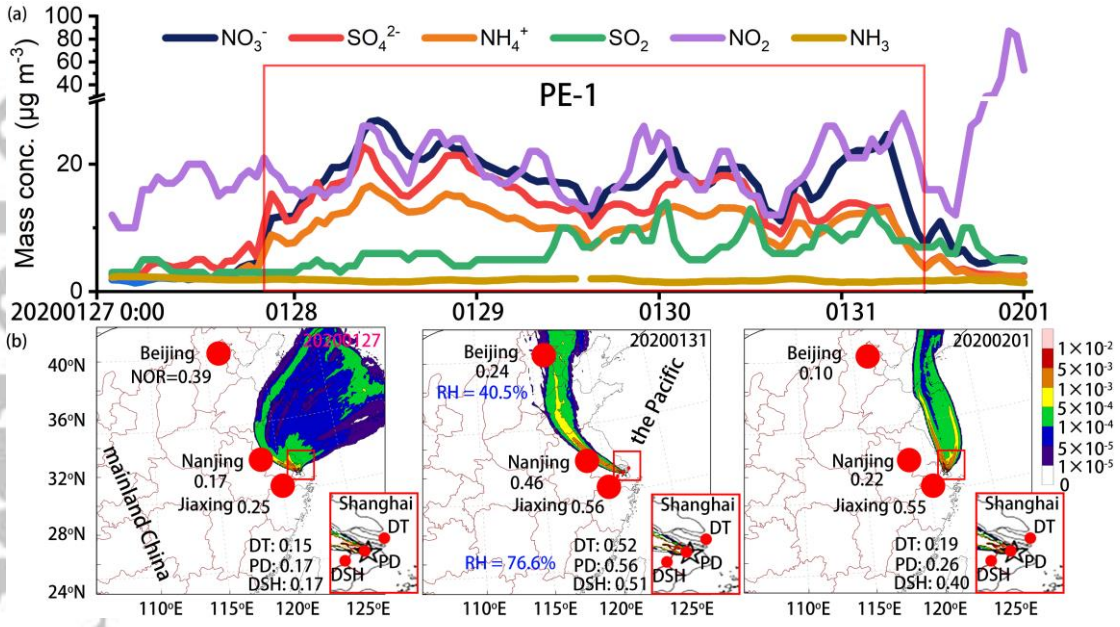

Figure 4. (a) Time series of the mass concentrations of SNA and their gaseous precursors at PD in Shanghai from 00:00 January 27 to 00:00 February 1 (local time). The red frame outlines the period of pollution episode PE-1. (b) 48 h air mass back-trajectories in Shanghai on January 27, January 31, and February 1. The footprint distributions of back-trajectories are shown in shaded colors. The expression of the date is yyyymmdd. The color bar displays the relative frequency of footprints, normalized to 1 (the color range has been limited to 0-0.02 to highlight grid points with low but a non-zero contribution). Numbers in black indicate NOR. Inset: The location of the three sites in Shanghai (DT, PD, and DSH).